High-Precision Position Control of a Novel Planar Switched Reluctance Motor

Jianfei Pan, *Student Member, IEEE*, Norbert C. Cheung, *Senior Member, IEEE*, and Jinming Yang

***Abstract*—This paper presents the position control of a novel two-dimensional (2-D) switched reluctance (SR) planar motor. The planar motor consists of a six-coil moving platform and a flat stator base made from laminated mild steel blocks. Unlike conventional $x-y$ tables, which stack two moving slides on top of each other, the proposed 2-D planar motor has the advantages of simple mechanical construction, high reliability, and the ability to withstand harsh operating conditions. Together with the two linear encoders attached to the x-axis and y-axis, the motor can be controlled under closed-loop mode. To combat the problem of force nonlinearity, this paper proposes a cascade controller with force linearization technique to implement the drive controller. Due to the unique structure of the planar motor's magnetic circuit, there is very little coupling between the x-axis and y-axis, and no decoupling compensation is needed. Preliminary results show that the proposed SR planar motor has a positional accuracy of 5 μm and a maximum acceleration/deceleration rate of 2 G.**

***Index Terms*—Planar motor, position control, switched reluctance.**

I. Introduction

IN THE INDUSTRY, precise motion control for two dimensions is in high demand. This is often achieved by employing dc or ac motors as the prime motion actuator and by coupling their output shafts to mechanical motion translators (e.g., reduction gear, belt, ball screw, etc.) with mechanical slides, stacked on top of each other to form an $x-y$ table. Though this is the most widely used method, it has disadvantages of reduced accuracy, complex mechanical structure, difficult adjustments and alignments, high production cost, low reliability, etc.

To overcome the above problems, a few direct-drive planar solutions have been proposed.

Sawyer motor [1], [2] is the first and the only practical type of planar motor available in the industry. Though it can provide uniform performance over the entire workspace and offer fairly high speeds, its open-loop nature is susceptible to the loss of steps when it is subject to external disturbances.

Planar motors based on permanent magnets are proposed in [3]–[5]. In [3], permanent magnets are located in the base and organized as a checkerboard arrangement. The mover has eight coils installed on two linear guides. Another scheme [4], [5] shows an intercalated arrangement of coils for the moving platform, and the mover is composed of two high-energy permanent magnets fixed on trucks. Planar motors based on permanent magnets have complicated structures, and the utilization factor of the magnets is very low. Besides, the manufacturing and maintenance costs are high and complex.

In this paper, a novel planar motor based on the switched reluctance (SR) principle is introduced [6]. The manufacturing cost of SR actuator is much lower than that of similar permanent magnetic devices. The proposed actuator has a very simple structure with very few mechanical parts. Thus, this planar motor can be manufactured easily. Since the motion system is a self-aligned direct-drive system, there is no need for $x-y$ alignments or rotary-to-linear couplings.

At present, linear motion systems based on the SR principle are mainly focused on transportation systems and their control target is on the regulation of velocity. Recently, a linear SR actuator that is targeted toward high-precision position control has been developed in our laboratory [7], [8]. This linear SR motor can achieve 1-μm precision and 2.5-G acceleration rate. The construction of a direct-drive two-dimensional (2-D) SR planar motor is a continuous extension from the previous idea.

The purpose of this paper is to describe the characteristics and modeling of the planar SR motor and the construction of a nonlinear cascade controller for the motor. The organization of this paper is as follows. The design and construction of the planar motor are introduced in Section II. Section III focuses on the motor's electrical and control characteristics. In Section IV, a cascade control scheme with nonlinear lookup tables is proposed. Section V describes the implementation of the planar SR motor drive system and the results obtained.

II. Construction of the Planar Motor

Fig. 1 shows the overall structure of the planar SR motor. It is based on the "straightened-out" version of a 6/4-pole rotary SR motor along the x-axis and y-axis. Since the motor is 2-D, the stator plate consists of square extrusion blocks instead of a rectangular extrusion toothed rail, as in the case of most linear SR motors. Two roller slides are employed to support movement in the x-axis, and another pair of linear guides is attached to the base to enable the motor for movement in the y-axis.

Instead of carving the square extrusions from a single slab of steel, the base plate is constructed from small pieces of "laminated steel blocks," as shown in Fig. 2(a) and (b). The blocks

Manuscript received June 29, 2004; revised November 22, 2004. Abstract published on the Internet September 26, 2005. This work was supported by the Hong Kong Research Grants Council under Project Code B-Q473.

J. Pan and N. C. Cheung are with the Department of Electrical Engineering, Hong Kong Polytechnic University, Kowloon, Hong Kong (e-mail: eencheun@inet.polyu.edu.hk).

J. Yang is with the Department of Electrical Engineering, Electrical Power College, South China University of Technology, Guangzhou, China (e-mail: jmyang@scut.com.cn).

Digital Object Identifier 10.1109/TIE.2005.858708

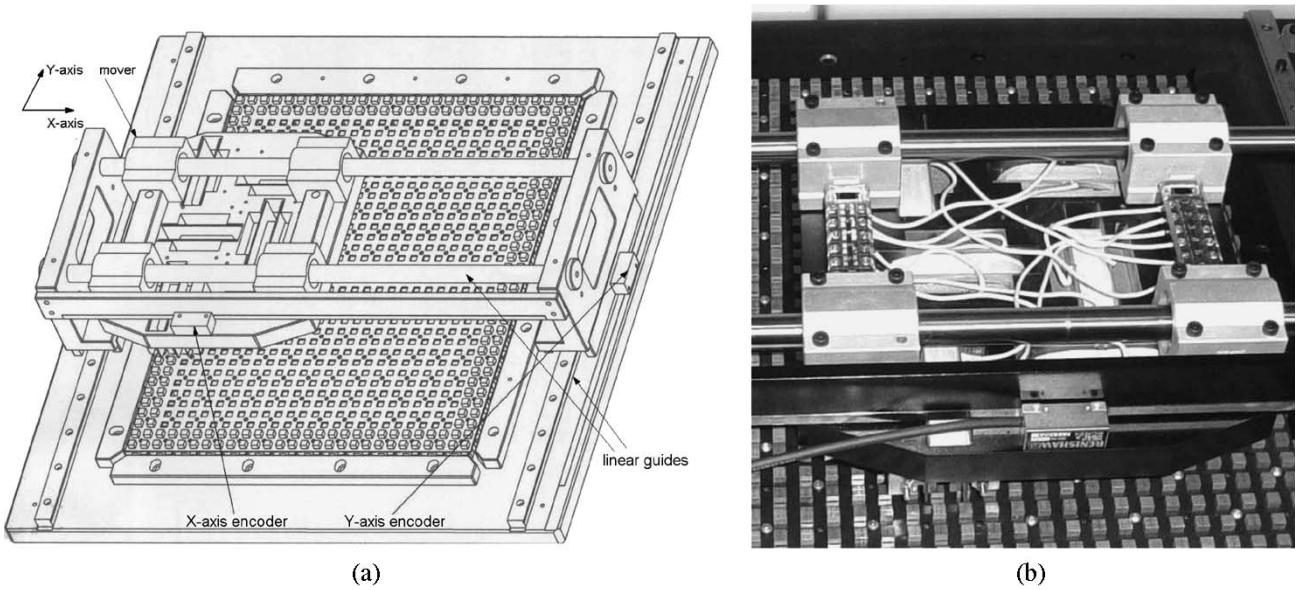

Fig. 1. Planar SR motor. (a) Overall diagrammatic view. (b) Close-up view of the actual moving platform.

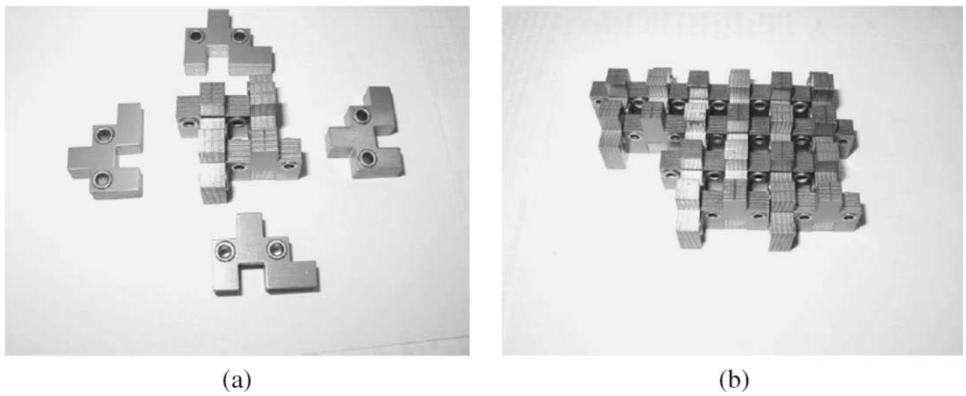

Fig. 2. Construction of the stator base. (a) Individual laminated steel blocks making up the stator. (b) Grouping the blocks together to form the base of the stator.

are held together by epoxy glue. This method of construction can reduce the manufacturing cost and simplify the overall construction complexity. Since the blocks are laminated, it can reduce the eddy-current effect in the magnetic circuit. Moreover, the same laminated blocks can be used to construct different sizes of base plates, according to different requirements and applications.

Two sets of three-phase coil windings with wide magnetic teeth are employed on the moving platform. Altogether there are six coils, with three coils responsible for each direction. Fig. 3(a) and (b) shows the three-dimensional (3-D) view and the side view of this magnetic circuit arrangement. All six coils have the same dimensions and ratings. The thickness of the laminated plates on the moving platform is chosen to be a multiple of the motor's pole pitch. This arrangement allows the total overlap air gap area remain unchanged for any perpendicular movement of the platform. Therefore, the three coils will generate force in one direction only. Since the moving platform contains two sets of three phase coils, perpendicular to each other, each set of coil will generate force in one direction only, and the two axes are forced decoupled from each other. Two sets of three-phase flux decoupled winding arrangement with longitudinal configuration are chosen because it has the following advantages [7], [9].

1) The decoupled flux windings lead to a simpler motor model due to zero mutual inductance.
2) The individual phase windings reduce the manufacturing cost and complexity.
3) Long travel distance can be accomplished easily by combining longitudinal track guides.

Table I lists the major dimensions and parameters of the planar SR motor. In the investigation, a motor with a traveling range of 300 $\times$ 300 mm was constructed. However, the base plate is made up of small pieces of "laminated steel blocks." Therefore, the motor can be easily constructed to different sizes based on the same principle and calculations.

III. Electrical and Magnetic Characteristics

In this section, the electrical characteristic of the planar motor is developed from its voltage equation. Then, the force characteristics and the flux linkage behavior of the planar motor

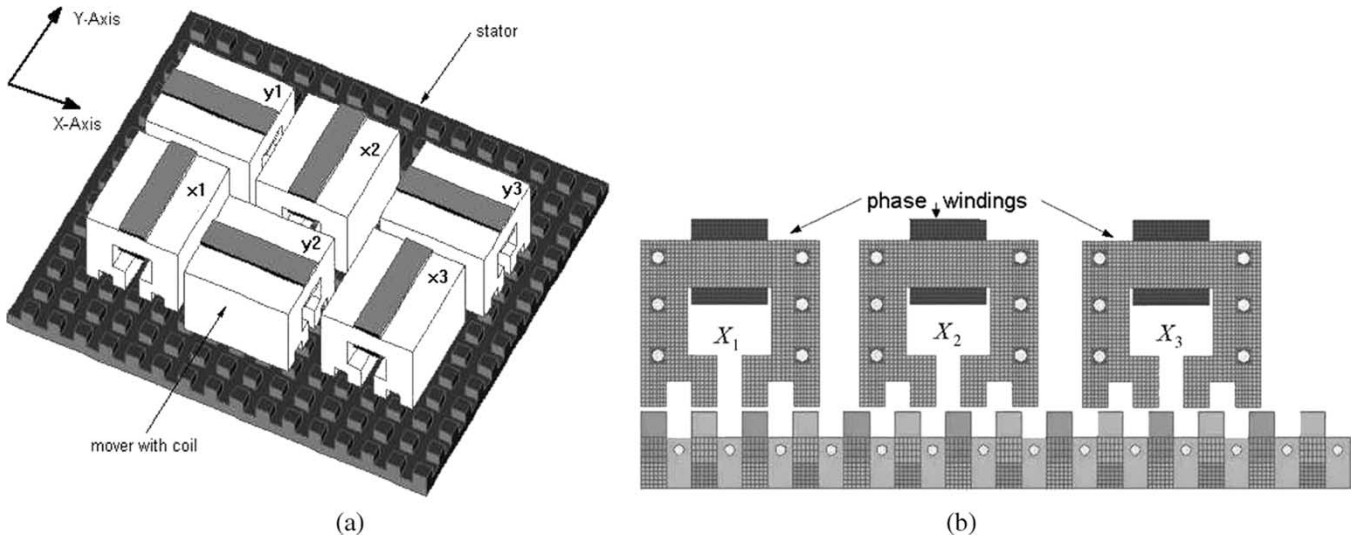

Fig. 3. Magnetic circuit of the SR planar motor. (a) 3-D view. (b) Side view.

are investigated. For this purpose, the flux linkage profile of the planar motor is measured from the actual hardware. After this, the sparse flux linkage data are joined together to form a 3-D profile by using an appropriate curve fitting method.

Equation (1) shows the general voltage equation of the planar SR motor. Since the two axes are considerably decoupled, either axis can be controlled independently, and the nonlinear equations governing the SR motor can be applied to both axes.

For the Kth phase of one axis

$$V_k(t) = R_k i_k(t) + \frac{\partial \lambda_k\left(i_k(t), x(t)\right)}{\partial x(t)} \frac{\mathrm{d}x(t)}{\mathrm{d}t} + \frac{\partial \lambda_k\left(i_k(t), x(t)\right)}{\partial i_k(t)} \frac{\mathrm{d}i_k(t)}{\mathrm{d}t}$$
$$\lambda_k = \lambda_{kj} + \lambda_{km} + \lambda_{ke} \tag{1}$$

where $V_k(t)$, i_k, and R_k are the phase voltage, phase current, and phase resistance, respectively. $x(t)$ and λ_k stand for the position and the total flux linkage. The flux linkage λ_k composes of self-flux λ_{kj}, mutual flux λ_{km}, and leakage flux linkage λ_{ke}.

The force equations are

$$\begin{aligned} f_{x(y)}&\left(i_a(t), i_b(t), i_c(t), x(t)\right) \\ &= \sum_{k=a}^{c} \frac{\partial \int_0^{i_k(t)} \lambda_k \mathrm{d}\tau_k(t)}{\partial x(t)} \\ &= \sum_{k=a}^{c} f_k\left(i_k(t), x(t)\right) \\ &= M_m \frac{\mathrm{d}^2 x(t)}{\mathrm{d}t^2} + Bv \frac{\mathrm{d}x(t)}{\mathrm{d}t} + f_l(t) \end{aligned} \tag{2}$$

where $f_{x(y)}$ is the totally generated electromechanical force of one axis, $f_{l(t)}$ is the external load force, and M_m and B_v are the mass and the friction constant, respectively.

In the measurement of flux linkage, the profile is measured using the "search coil" method [10], [11]. An ac current from an isolated autotransformer ranging from 0 to 50 A is fed into the main coil. By measuring the induced voltage across the search coil, flux can be calculated according to

$$\varphi(t) = -\frac{1}{N_s} \int e(t) dt \tag{3}$$

where $e(t)$ is the voltage induced by the flux and N_s is the number of the search coil.

Then flux linkage is calculated as

$$\lambda(t) = N_1 \varphi(t) \tag{4}$$

where N_1 is the number of turns of the main coil.

Fig. 4 shows the flux linkage hysteresis loops at different positions and current levels. The maximum shift of flux linkage is around 0.2 Wb, which means there is about $\pm 10\%$ change from the total flux linkage. Actually, for most of the time, the motor operates well below its rated current value, and there is very little chance that the current change will go from positive maximum to negative maximum. Under this circumstance, the hysteresis effect will not put a heavy burden on the current controller. Therefore, a hysteresis controller is not required.

TABLE I
MAJOR PARAMETERS OF THE PLANAR MOTOR

Pole pitch	6 mm
Air gap	0.55mm
Number of turns per phase	160
Rate power	120W
Phase resistance	1.5Ω
Size of base plate	450×450mm
Travel distance	300×300mm
Mover size	250×220mm
Encoder precision	0.5 μm

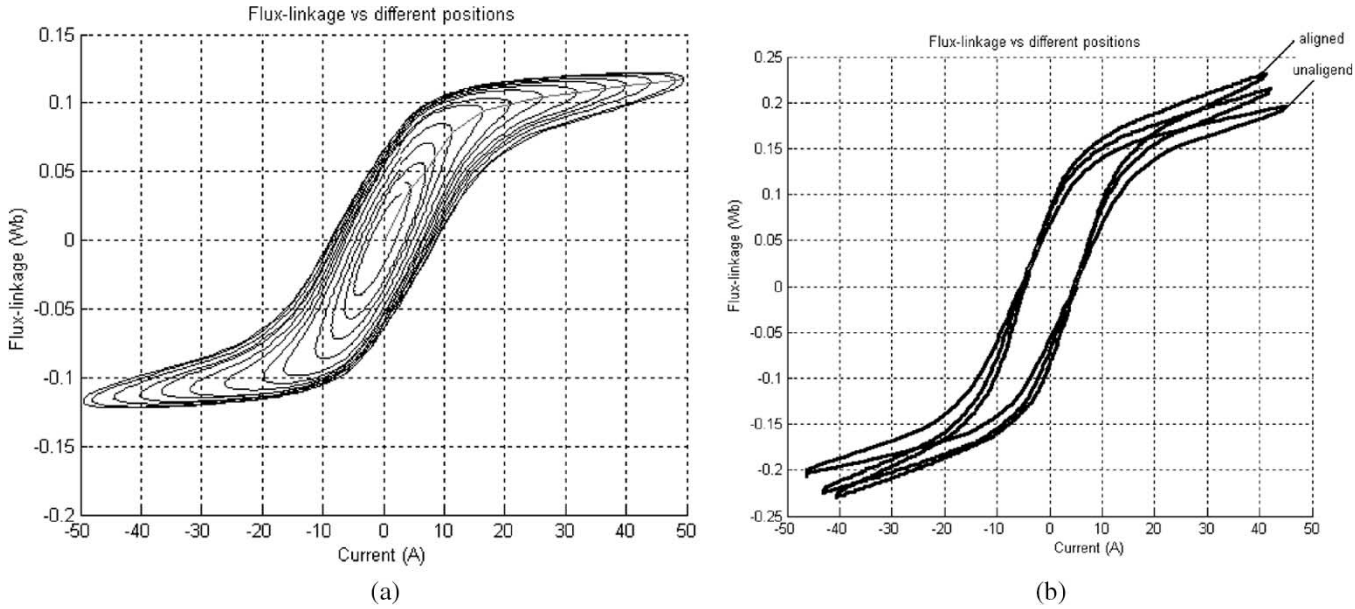

Fig. 4. Hysteresis loops of the magnetic circuit (a) at different currents and (b) at different positions.

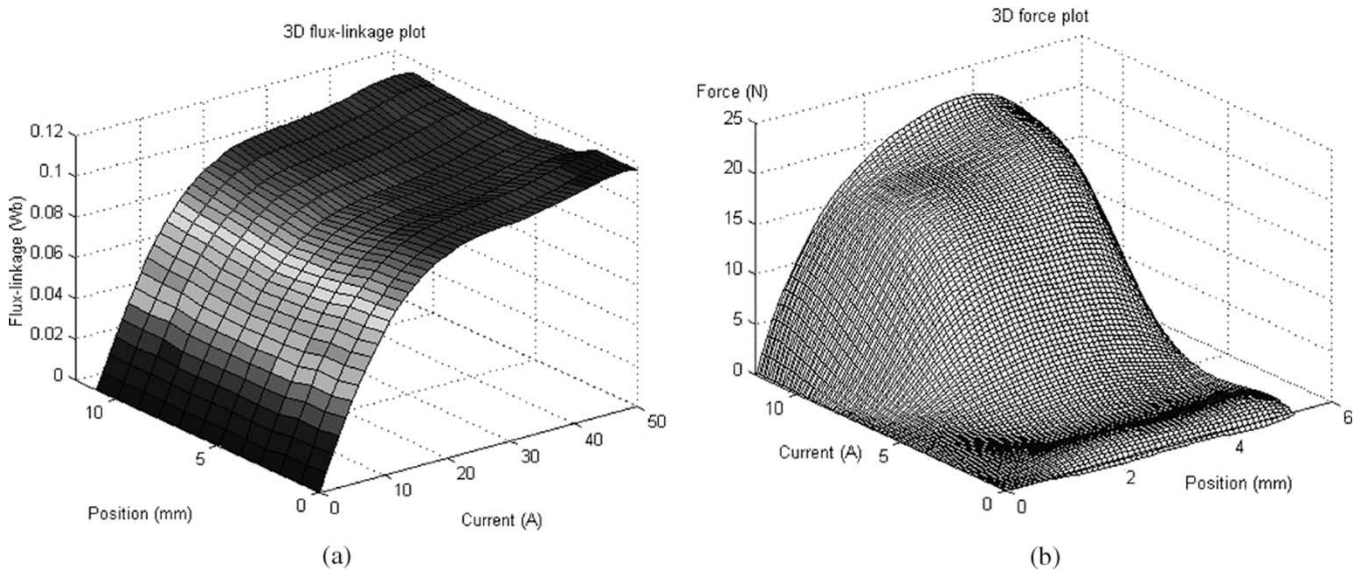

Fig. 5. Characteristics of the SR planar motor. (a) Flux linkage versus current and position. (b) Force versus current and position.

To obtain flux linkage profile, the vertex points on the positive side of the hysteresis loops are joined together and a 3-D plane is formed. The resultant flux linkage profile versus current and position is shown in Fig. 5(a). In the graph, the intermediate points are deduced by fourth-order polynomial curve fitting for the x-axis and y-axis using the equation shown in (5). This curve fitting method produces a tolerance less than 0.1%, i.e.,

$$f(x,y) = \sum_{n=1'}^{4} \sum_{m=1}^{4} C_{n,m} x^n y^m. \tag{5}$$

The next important set of parameter for the motor is the force output at different positions and current levels. This set of data is obtained by direct measurement. To achieve accurate measurement precisely at each of the predetermined locations, a test rig fixture is constructed, which can accurately divide one pole width (6 mm) into 50 different equally spaced divisions. Once the moving platform is fixed into place, different current values (0–25 A) are injected into the phase winding. After this, the motor's force is measured by a load cell sensor, which then feeds the force value directly to the computer. Since the phase windings are magnetically decoupled and the mechanical parameters are identical, only one phase of measurement is needed. Fig. 5(b) shows the 3-D plot of force versus current and position.

IV. Control Strategy

Due to the unique structure of the planar SR motor, the two axes are virtually decoupled from each other. Under this circumstance, two individual controllers are used to control the

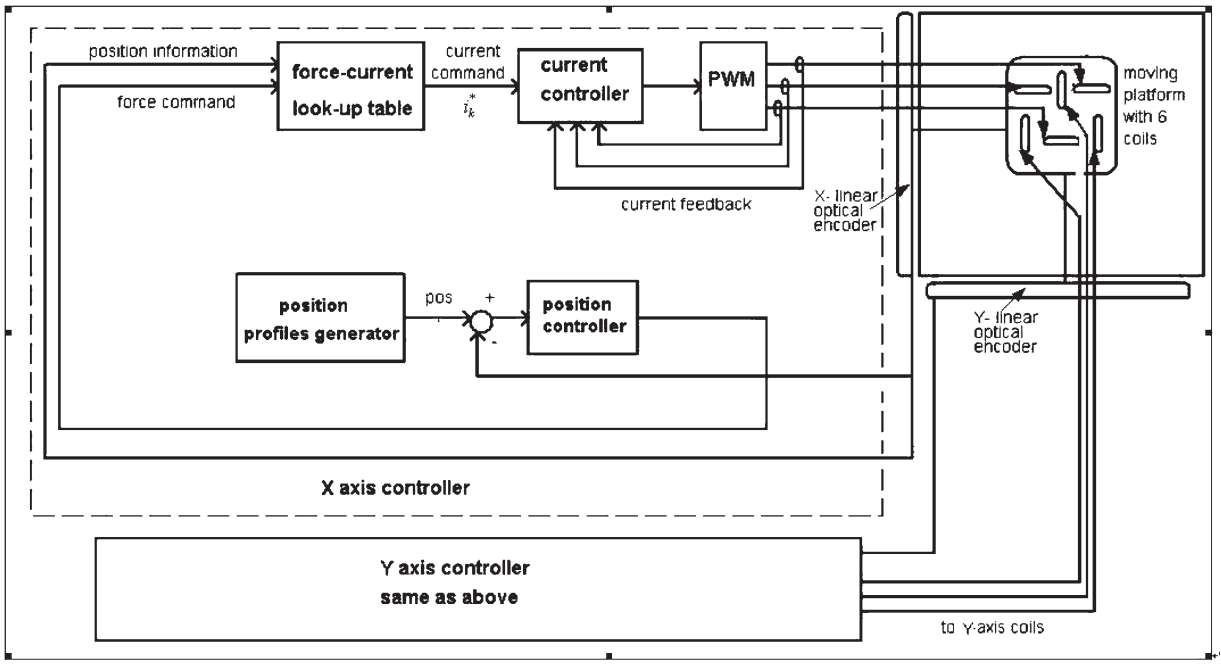

Fig. 6. Overall block diagram of the controller.

TABLE II
PHASE EXCITATION TABLE (0 mm = PHASE A AT FULLY ALIGNED POSITION)

Region	Position range(mm)	+ve force command	-ve force command
1	0—2	B	C,A
2	2—4	B,C	A
3	4—6	C	A,B
4	6—8	C,A	B
5	8—10	A	B,C
6	10—12	B,A	C

two axes of the motor. Fig. 6 shows the overall block diagram of the control system.

Exploiting the fact that the current dynamics are at least an order faster than the mechanical response, this paper proposes a dual rate cascade control approach. A fast inner loop current controller is employed to regulate the current–voltage nonlinearity of the actuator while a slower outer loop position controller is used to control the mechanical dynamics. On top of this, a nonlinear function is included to compensate the nonlinearity of force against current and position.

A. Current Controller

The relationship between the output current and the input voltage for one phase of SR motor is represented as [8]

$$\dot{i}_k = -\frac{R}{L_k(x,i)} i_k - \frac{\partial L_k(x,i)}{\partial x}\dot{x}\frac{1}{L_k(x,i)} i_k + \frac{1}{L_k(x,i)} V_k \tag{6}$$

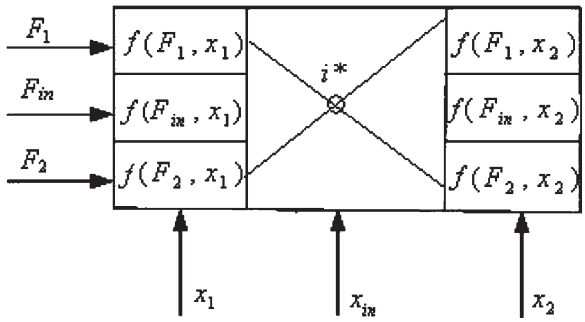

Fig. 7. Calculation of current from force/position through the lookup table.

where i_k is output current, V_k is input voltage, R is the winding resistance, and $L_{k(i)}$ is the inductance.

At the side of the pulsewidth modulation (PWM) drive, the relationship between output and input is

$$\dot{i}_k = -\frac{R}{L_k(x)} i_k + \frac{C}{L_k(x)} U_k \tag{7}$$

where C is the converter gain and U_k is the controller input.

From Fig. 5(a), it can be seen that there is little variation of flux linkage with respect to position change. The graph also shows that the gradient of flux linkage remains relatively constant from 0 to 20 A before it enters the saturation region. Even in the saturation region, the gradient of flux linkage gently declines in a uniform fashion. Through this inspection, a simple PD current controller is proposed. The reduction in the flux linkage gradient is merely treated as a disturbance and can be regulated quite easily in the PD control. The equation governing the controller is

$$U_k = \frac{L_k(x,i)}{C}\left(\frac{R_k}{L_k(x)} i_k + \frac{\mathrm{d}i_k^*}{\mathrm{d}t} + K_p\left(i_k^* - i_k\right)\right) \tag{8}$$

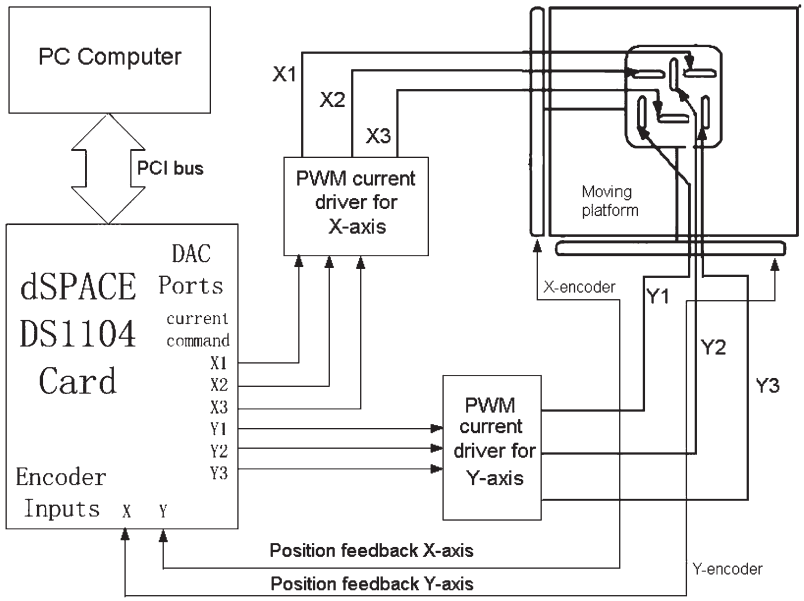

Fig. 8. Experiment setup of the whole system.

where i_k^* is the converter gain and $L(x,i)$ is the inductance or the gradient of flux linkage versus current. These values can be obtained from Fig. 5(a). Kp is a constant value. Let $e = i_k^* - i_k$, and substitute (8) into (7), yielding

$$\dot{e} + K_p e = 0. \tag{9}$$

By choosing a proper value of Kp, the error e will diminish to zero within a relatively short time. By limiting the rise time to 180 Aμs^{-1} for the current controller, an overshoot free response can be achieved.

As long as the current controller can track the current command much faster than the outer position control loop, the outer position loop will have no difficulty in controlling the overall position of the planar motor.

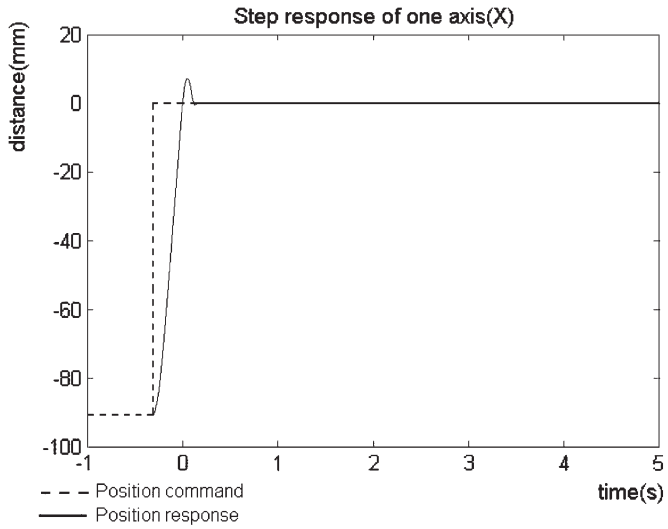

Fig. 9. Step response of the position controller.

B. Nonlinear Force to Current Lookup Table

The nonlinear relationship between output force and flux linkage is described in Fig. 5(b). In the controller, an inverse force function is needed to output the current command to the drivers from the inputs of force and position. There are several options to implement this nonlinear function:

1) by using polynomial or bicubic spline curve-fitting technique [12];
2) by using a 2-D lookup table [13];
3) by implementing a neural network [14].

The polynomial curve-fitting method requires the least memory but involves complex calculations, especially in the 2-D calculation case. The bicubic spline strategy can be more precise if the order of approximation is high. However, higher-order computation requires more computational effort because there are many matrix coefficients needed to be calculated online. The second method is the fastest and requires the least computation, but the memory requirement maybe very large if a high-resolution output is required. The last method also involves heavy computation load. It is best used for learning unknown nonlinear functions. In this case, the lookup table is fully defined; therefore, there is no need for a neural network.

To optimize between computation efficiency and memory consumption, this paper uses low-resolution 2-D lookup tables for each axis of motion with bilinear interpolation to calculate the intermediate values.

The nonlinear force to current lookup table consists of two stages. The first stage is to resolve the total force command from the position controller output into three components for each phase, fa, fb, and fc. Then the second stage is responsible for calculating three desired phase currents ia, ib, and ic from the force components of fa, fb, and fc accordingly.

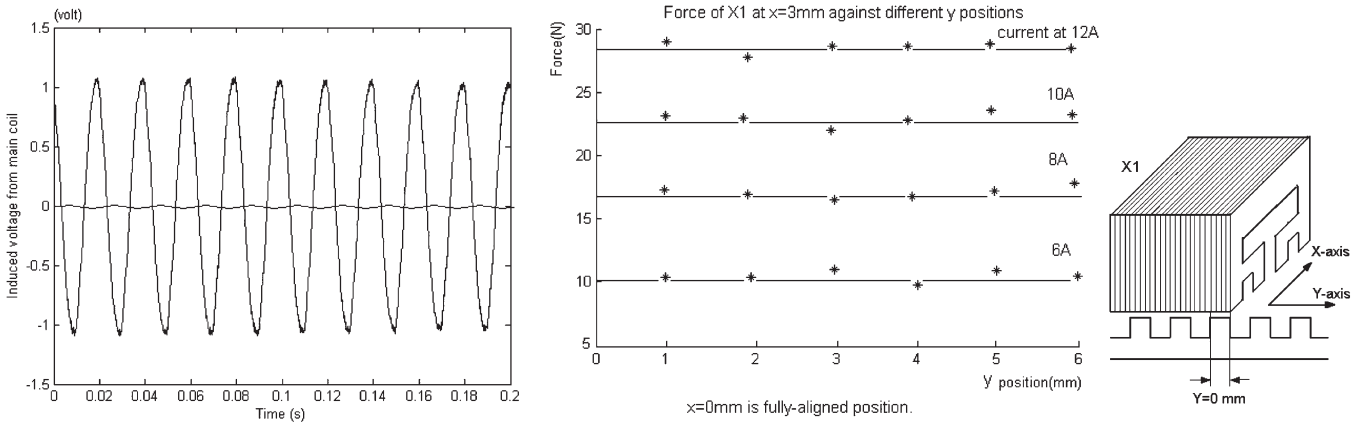

(a) (b)

Fig. 10. Coupling effect between the x-axis and y-axis. (a) Induced voltage between the closest x and y windings. (b) Force variation on the x-axis when the coil is moving along the y-axis.

For each direction, the region decision mechanism is employed to generate the three-coupled force command. Table II illustrates which phase(s) should be excited according to current mover position. For example, if the position falls into region 5 and the required force command is a negative value, then phases B and C will be energized to produce the required force; on the contrary, if the force command is a positive value, then only phase A will be energized to generate the total command force. Here, a simple linear force distribution method is used if the two phases are simultaneously excited.

Since the relations of force, current, and position are nonlinear in nature, a 2-D force current position lookup table for each axis is used to describe the nonlinear force profile. To find out the inverse relationship between current, force, and position, another experiment has been conducted by fixing the moving platform at the corresponding 50 positions within one pole width, and then currents are measured to generate the desired force. Alternatively, the table can be generated from the inverse function of force versus current and position, as described in Fig. 5(b).

Fig. 7 shows the method of obtaining the required current i^* by bilinear interpolation method. First, from the position input x_{in} and force command F_{in}, two pairs of data $f(F_1, x_1)$ and $f(F_2, x_1)$ in the lookup table are located. For each pair, a linear interpolation is done according to the ratio of F_1, F_2, and F_{in}. As a result, two intermediate elements $f(F_{1-2}, x_1)$ and $f(F_{1-2}, x_2)$ can be obtained. Finally, the output current command i^* is obtained by interpolating the two intermediate elements with x_1, x_2, and x_{in}.

For the implementation of the inverse force current position lookup tables, continuity and smoothness of the profile are more important than accuracy. Therefore, we use relatively low 27 $\times$ 27 elements to build up the lookup table for the force compensation values. To ensure the smoothness, a 2-D linear interpolation scheme is implemented for the intermediate values. This produces a considerably low worst-case deviation from the original nonlinear function and the output values can also follow a smooth profile. A 27 $\times$ 27 element lookup table with 2-D linear interpolation is sufficient to describe the force profile with an accuracy of $\pm 5\%$.

C. Position Controller

The position controller forms the essential part of the slow subsystem. Its operation is based on the assumption that the current controller has perfect tracking capability and the force-to-current lookup table generates the linearized current command to the current controller. The dynamics of the planar SR motor can be represented as a second-order mechanical system

$$M(S) = \frac{1}{S(M_m S + B_v)} \tag{10}$$

where M_m is mover mass and B_v is the combined friction coefficient of motor and load. For this linear system, a simple proportional–integral differential (PID) controller is already sufficient, it has the form of

$$u = \left(\frac{K_i}{S} + K_d S + K_p\right) \text{err}(S) \tag{11}$$

where err(S) and u are controller input and output, respectively. K_d, K_p, and K_i are the derivative, proportional, and integral gains, respectively. By properly choosing appropriate gain values, the whole system is stable and the motor can reach a high precision. The gain parameters are selected according to the second-order dynamic response of the system. They are further fine tuned by repeated trial and error.

V. Implementation and Results

The experiment is implemented on a dSPACE DS1104 DSP motion controller card. This card has an on-board 250-MHz DSP for real-time computation and interfaces with the PC through the peripheral component interconnect (PCI) bus. It consists of two channels of 24-bit incremental encoder inputs, six channels of 12-bit analog input, and six channels 12-bit analog output. The control card can directly interface with Real-Time Workshop and MATLAB, and control parameters can be modified online. Fig. 8 is the overall experiment setup. Knowing the fact that the outer position loop bandwidth is often in the order of hundreds of hertz and the inner current loop is

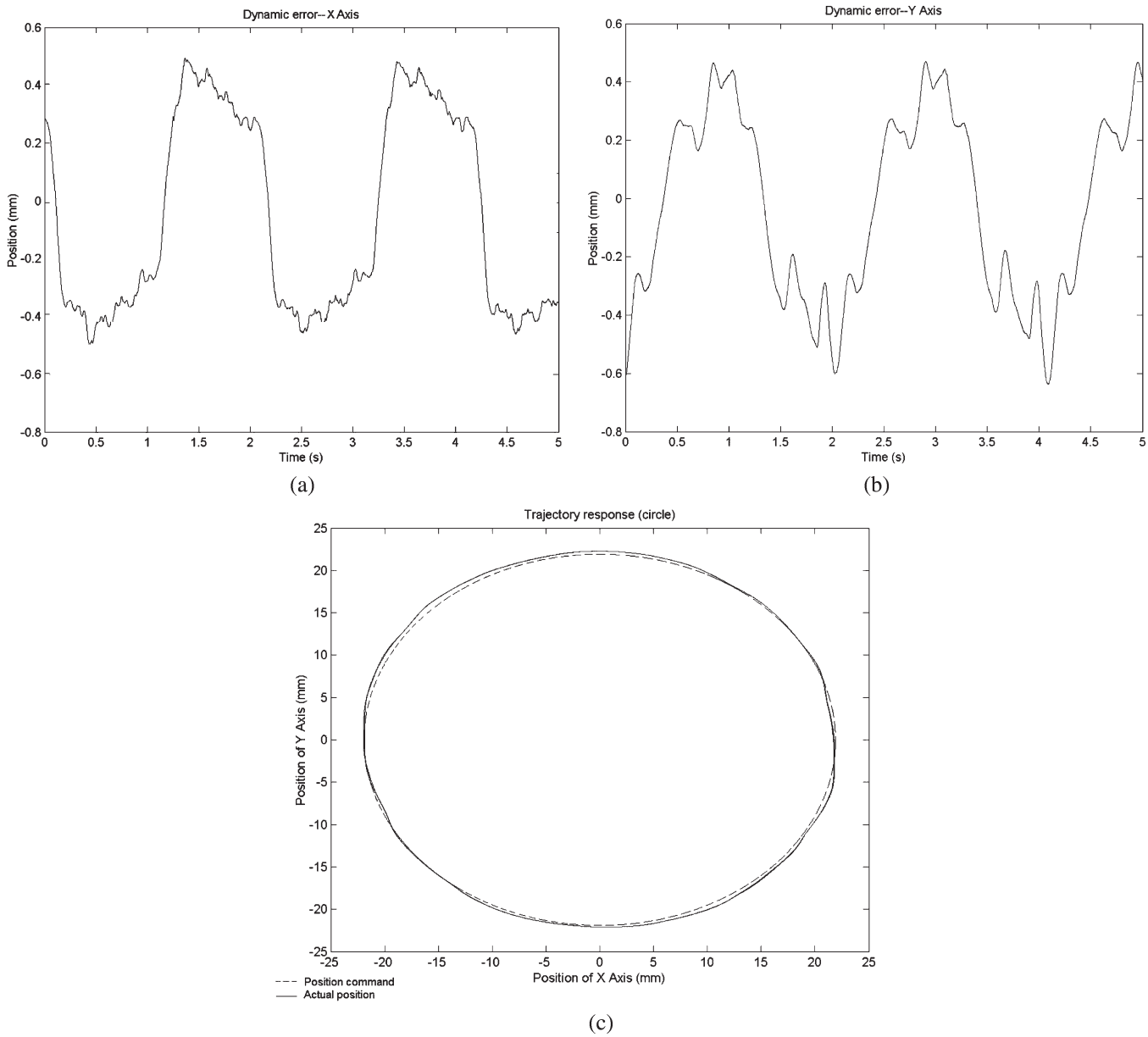

Fig. 11. Trajectory response of the planar SR motor for circular motion. (a) Tracking error of the x-axis (y in millimeter, x in second). (b) Tracking error of the y-axis (y in millimeter, x in second). (c) Overall 2-D trajectory path (y in millimeter, x in millimeter).

significantly faster, a sampling rate of 10 kHz is selected for the inner loop. Since the bandwidth of the mechanical moving parts of the planar motor is in the order of 100 Hz, the outer loop's sampling rate of 2 kHz is already more than sufficient.

Fig. 9 shows the step response of one position controller. The settle time for a 90-mm step response travel is 0.8 s and the position error is virtually zero.

To ensure that two axes of motion can be controlled individually, several experiments on inter-axis coupling have been conducted. It is found that the force of each axis contributes to less than 1% of that of the other; therefore, the problem of inter-axis coupling force is considered insignificant and can be easily corrected by the controller of each axis. Fig. 10(a) shows the output voltage from an x-axis coil when its nearby y-axis coil is excited with a sinusoidal voltage. The output of the y-axis coil is virtually zero. Fig. 10(b) shows the force variation of the moving platform along the y-axis when it is measured at different points of the x-axis. Again, the variation is virtually zero. These results confirmed that the inter-axis coupling of this unique planar motor structure is very small.

Fig. 11 shows the performance of the motor when it is drawing a circle. Overall, the motor can track a circular trajectory path satisfactorily. However, the dynamic error of some places can be as high as 0.5 mm. This is due to the uneven mechanical friction of the prototype; it can easily be improved in the second version. Due to the structure of the support mechanics, the effective mass of mover for the two axes is different; therefore, the dynamic responses for the two axes are also different. The dynamic error of the y-axis is consistently larger than the x-axis.

When a maximum current of 20 A is injected into the coils, a maximum acceleration of 2 G can be achieved. For

point-to-point repeatability, an accuracy of 5 μm is achieved. This kind of performance is already quite excellent for the first prototype.

VI. Conclusion

This paper has described the development of a two-dimensional (2-D) motion system based on a novel planar switched reluctance (SR) motor. The motor has a very simple construction and can withstand harsh environments. The manufacturing procedure for the 2-D SR planar motor is simple and straightforward. The motor consists of a moving platform that houses six coil windings that can be made by coil winding machine individually. The base plate is constructed from small pieces of laminated blocks that can be mass produced cheaply and easily. Moreover, there is no need for costly and difficult-to-handle motor components like magnets, commutators, or complex overlap windings.

In this project, a cascade controller with 2-D linearization tables is employed to produce precise and uniform force output for the planar SR motor. Due to the innovative design of the motor, there is very little cross coupling between the x-axis and y-axis; therefore, a force decoupler is not necessary for the control of the planar motor. Preliminary results show that the motor can be controlled to a positional accuracy of 5 μm and an acceleration rate of 2 G under normal load. The proposed planar SR motion system is therefore an ideal replacement for traditional $x-y$ tables in industrial automation applications.

References

[1] B. A. Sawyer, "Magnetic positioning device," U.S. Patent 3 457 482, Jul. 22, 1969.

[2] E. R. Pelta, "Two-axis Sawyer motor for motion systems," *IEEE Control Syst. Mag.*, vol. CSM-7, no. 5, pp. 20–24, Oct. 1987.

[3] D. Ebihara and M. Watada, "Study of a basic structure of surface actuator," *IEEE Trans. Magn.*, vol. 25, no. 5, pp. 3916–3918, Sep. 1989.

[4] A. F. Flores, A. A. Susin, and M. A. da Sliveira, "Application of Neodymium-Iron-Boron permanent magnets on the assembling of a novel planar actuator," *IEEE Trans. Magn.*, vol. 35, no. 5, pt. 2, pp. 4034–4036, Sep. 1999.

[5] J. Tsuchiya and G. Kimura, "Mover structure and thrust characteristic of moving-magnet-type surface motor," in *Proc. IEEE IECON'01*, vol. 2, Nov. 29–Dec. 2 2001, pp. 1469–1474.

[6] N. C. Cheung, J. F. Pan, and J. M. Yang, "Two dimensional variable reluctance planar motor," U.S. Patent LUNGBJ/101/US, May 6, 2004.

[7] W. C. Gan and N. C. Cheung, "Development and control of a low-cost linear variable reluctance motor for precision manufacturing automation," *IEEE/ASME Trans. Mechatronics*, vol. 8, no. 3, pp. 326–333, Sep. 2003.

[8] W. C. Gan, N. C. Cheung, and Q. Li, "Position control of linear switched reluctance motors for high precision applications," *IEEE Trans. Ind. Appl.*, vol. 39, no. 5, pp. 1350–1362, Sep./Oct. 2003.

[9] C. T. Liu and J. L. Kuo, "Experimental investigation and 3-D modelling of linear variable-reluctance machine with magnetic-flux decoupled windings," *IEEE Trans. Magn.*, vol. 30, no. 6, pp. 4737–4739, Nov. 1994.

[10] T. J. E. Miller, *Switched Reluctance Motor and Their Control*. Oxford, U.K.: Clarendon, 1993.

[11] K. K. C. Chan and N. C. Cheung, "Modelling and characterisation of a novel two-finger variable reluctance gripper," *ISA Trans.*, vol. 44, no. 2, pp. 177–185, Apr. 2005.

[12] X.-D. Xue, K. W. E. Cheng, and S. L. Ho, "Simulation of switched reluctance motor drives using two-dimensional bicubic spline," *IEEE Trans. Energy Convers.*, vol. 17, no. 4, pp. 471–477, Dec. 2002.

[13] J. M. Stephenson and J. Corda, "Computation of torque and current in doubly salient reluctance motors from non-linear magnetization data," *Proc. Inst. Elect. Eng.*, vol. 126, no. 5, pp. 393–396, May 1979.

[14] W. Lu, A. Keyhani, H. Klode, and A. B. Proca, "Modeling and parameter identification of switched reluctance motors from operating data using neural networks," in *Proc. IEEE Int. Electric Machines and Drives Conf. (IEMDC)*, Madison, WI, Jun. 2003, vol. 3, pp. 1709–1713.

Jianfei Pan (S'03) was born in Harbin, China, in 1978. He received the B.S. degree in electrical engineering from ChangChun University of Science and Technology, ChangChun, China, in 2001. He is currently working toward the Ph.D. degree in the Department of Electrical Engineering, Hong Kong Polytechnic University, Kowloon, Hong Kong.

His main research interest is the control of switched reluctance devices.

Norbert C. Cheung (M'91–S'95–SM'05) received the B.Sc. degree from the University of London, London, U.K., the M.Sc. degree from the University of Hong Kong, Hong Kong, and the Ph.D. degree from the University of New South Wales, Sydney, Australia, in 1981, 1987, and 1995, respectively.

He is currently with the Department of Electrical Engineering, Hong Kong Polytechnic University, Kowloon, Hong Kong. His research interests are motion control, actuator design, and power electronic drives.

Jinming Yang received the B.Sc. degree from the Beijing University of Aeronautics, Beijing, China, the M.Sc. degree from Zhejiang University, Zhejiang Province, China, and the Ph.D. degree from South China University of Technology, Guangzhou, China, in 1987, 1990, and 2000, respectively.

He is currently a Lecturer at South China University of Technology. His research interests are machine drives and nonlinear control.